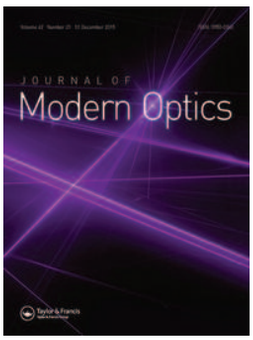

Journal of Modern Optics

ISSN: 0950-0340 (Print) 1362-3044 (Online) Journal homepage: http://www.tandfonline.com/loi/tmop20

Optical trapping Rayleigh dielectric particles with focused partially coherent dark hollow beams

Hua-Feng Xu, Wei-Jun Zhang, Jun Qu & Wei Huang

To cite this article: Hua-Feng Xu, Wei-Jun Zhang, Jun Qu & Wei Huang (2015) Optical trapping Rayleigh dielectric particles with focused partially coherent dark hollow beams, Journal of Modern Optics, 62:21, 1839-1848, DOI: 10.1080/09500340.2015.1045947

To link to this article: http://dx.doi.org/10.1080/09500340.2015.1045947

Journal of Modern Optics, 2015
Vol. 62, No. 21, 1839–1848, http://dx.doi.org/10.1080/09500340.2015.1045947

Optical trapping Rayleigh dielectric particles with focused partially coherent dark hollow beams

Hua-Feng Xu[a,b], Wei-Jun Zhang[a,b], Jun Qu[c]* and Wei Huang[a,b]*

[a]*Laboratory of Atmospheric Physico-Chemistry, Anhui Institute of Optics & Fine Mechanics, Chinese Academy of Sciences, Hefei, China;* [b]*School of Environmental Science & Optoelectronic Technology, University of Science and Technology of China, Hefei, China;* [c]*Department of Physics, Anhui Normal University, Wuhu, China*

(*Received 24 June 2014; accepted 22 April 2015*)

The focusing properties of coherent and partially coherent dark hollow beams (DHBs) through a paraxial *ABCD* optical system are theoretically investigated. It is found that the evolution behavior of the intensity distribution of focused partially coherent DHBs is closely related to their spatial coherence. The radiation forces (RFs) of focused coherent and partially coherent DHBs acting on a Rayleigh dielectric particle are also theoretically investigated. Numerical results show that the coherent and partially coherent DHBs can be focused into a tight focal spot, which can be used to stably trap a Rayleigh dielectric particle with high refractive index at the focus point. The influences of different beam parameters, including the spatial coherence, beam waist width, beam order, and hollow parameter of partially coherent DHBs, on the RFs and the trap stiffness are analyzed in detail. Finally, the stability conditions for effective trapping particles are also discussed.

Keywords: focusing properties; radiation force; trap stiffness; partially coherent dark hollow beam

1. Introduction

The ability to remotely trap and manipulate micron-sized particles by the radiation pressure of light is a subject of great interest. This new technology, called as optical traps or tweezers, was derived from the seminal works of Ashkin in 1986 [1]. Since then, this optical trap technology has been widely applied in various areas of science, particularly in physics, chemistry, and biophysical research, for example, trapping micro-sized dielectric or metallic particles [1–3], trapping and cooling atoms [4], trapping single aerosol [5,6], the study of molecules such as DNA [7], and so on. More recently, Li et al. have successfully achieved optical trapping and manipulation of flowing red blood cells in living animals and realized a non-contact micro-operation to clear the blockage of capillary with optical tweezers for the first time [8]. Thus, optical tweezers have been developed into a versatile and convenient tool in microscopic research [9].

It is well known that light carries both energy and momentum, and the radiation forces (RFs) are stemmed from the exchange of momentum and energy between photons and particles. Two types of RFs are identified in optical tweezers: the gradient force and the scattering/absorption force. The gradient force is responsible to pull the particle towards the center of the focus, while the scattering/absorption force tends to destabilize the trap. Thus, stable trapping requires the axial gradient force to dominate. In theory, three kinds of model have been developed to calculate the optical RFs in terms of the particle's size. The Rayleigh scattering model can be employed as a good approximation to the calculation of RFs acting on particles whose radius is much smaller than the wavelength of the incident beam [10]. For particles much larger than the wavelength of light, precise RF calculations can be carried out based on the ray optical model [11]. The *T*-matrix method provides an effective way for calculating the RFs on particles with size ranging from the Rayleigh regime to several wavelengths [12], and this method is also suitable for handling various realistically shaped particles [13]. It has been revealed that the RFs are closely related to the beam profile, the state of polarization, and coherence of the incident focused beam [2,12–21]. Up to now, the trapping characteristics of various types of fully coherent beams, such as elegant Hermite–cosine–Gaussian beams [14], pulsed Gaussian beams [15], Lorentz–Gaussian beams [16], abruptly autofocusing Airy beams [17], full Poincaré beam [18], cylindrical vector beams [2,12,19,20], and anomalous hollow beams [21] have been studied. However, in practice, any laser beam in laboratory is always partially coherent [22]. It has been revealed that partially coherent beams have advantages over the corresponding coherent beams for overcoming the destructive effect of the atmospheric turbulence [23]. Thus, it is of practical significance to incorporate partial coherence into beams and to investigate the influence of the spatial coherence length on the trapping effect. More recently,

*Corresponding authors. Email: qujun70@mail.ahnu.edu.cn (J. Qu); huangwei6@ustc.edu.cn (W. Huang)

numerous researchers have turned their attentions to partially coherent beams [24–28]. Wang et al. investigated the effect of spatial coherence on RFs acting on a Rayleigh dielectric sphere [24]. Zhao and Cai theoretically proposed a new method to trap two types of particles with different refractive indices by varying the spatial coherence of partially coherent elegant Laguerre–Gaussian beam [26].

Over the past several years, dark hollow beams (DHBs) with zero central intensity have attracted extensive interest due to their unique properties and wide applications in atom optics and modern optics [29–40]. A new controllable DHB model theoretically proposed by Cai et al. and Mei et al. can be expressed as a finite sum of Laguerre–Gaussian or Gaussian beams [32–34]. Propagation properties of various DHBs in turbulent atmosphere have been studied widely [32–38], and the tight focusing properties, such as the intensity distribution, the degree of polarization, and coherence, of partially coherent DHBs through a focusing system have also been investigated [39]. In the field of optical tweezing, it has been revealed that the focused dark hollow trap has some advantages over the conventional optical tweezers for minimizing photodamage on the trapped particle in experimental trapping [40]. However, as far as we know, the trapping characteristics of highly focused partially coherent DHBs on small particles have not yet been investigated. The present paper is devoted to the analysis of the RFs and the trap stiffness on a Rayleigh dielectric particle for the case where a focused partially coherent DHB is applied. The analytical formulas for the propagation of partially coherent DHBs through a paraxial *ABCD* optical system are derived in a tensor form. The focusing properties of coherent and partially coherent DHBs are numerically investigated. In addition, the effects of different beam parameters (i.e. the spatial coherence, the waist width, the beam order, and the hollow parameter) on the RFs and the trap stiffness are discussed in detail. Finally, the stability conditions for effective trapping particles are also analyzed.

2. Analytical formulas and the focusing properties of partially coherent DHBs through a paraxial *ABCD* optical system

In the rectangular coordinate system, the electric field of a DHB with circular symmetry at the input plane $z = 0$ can be expressed as a superposition of the electric field of a finite series of fundamental Gaussian modes as follows [33–36,38]

$$E_N(\boldsymbol{\rho}; z=0) = E_0 \sum_{n=1}^{N} \frac{(-1)^{n-1}}{N} \binom{N}{n} \left[\exp\left(-\frac{n\boldsymbol{\rho}^2}{w_0^2}\right) - \exp\left(-\frac{n\boldsymbol{\rho}^2}{w_p^2}\right) \right] \tag{1}$$

where E_0 is a constant related to the power of the incident beam, $\binom{N}{n}$ denotes a binomial coefficient, N is the beam order of a circular DHB. $w_p = pw_0$ with w_0 being the beam waist size of the fundamental Gaussian mode, p is a real positive parameter and must satisfies $p < 1$. The central dark size of the DHB can also be controlled by varying p, so we can call p as the hollow parameter. The area of the dark region of a DHB increases as N and p increase as shown in previous reports [33–36]. When $N = 1$ and $p = 0$, Equation (1) reduces to the expression for the electric field of a fundamental Gaussian beam. When $N > 1$ and $p = 0$, Equation (1) reduces to the expression for the electric field of a flat-topped beam [25]. Here, we assume the input power of the DHBs to be P_0 which is calculated by the following formula [10,25]

$$P_0 = \int_{-\infty}^{\infty} \int_{-\infty}^{\infty} I(\boldsymbol{\rho}; z=0)\,\mathrm{d}x\,\mathrm{d}y \tag{2}$$

where the intensity distribution can be expressed as

$$I(\boldsymbol{\rho}; z=0) = \frac{n_m \varepsilon_0 c}{2} |E_N(\boldsymbol{\rho}; z=0)|^2 \tag{3}$$

n_m is the refractive index of the surrounding medium, $c = 1/\sqrt{\varepsilon_0 \mu_0}$ is the speed of the light in vacuum, ε_0 and μ_0 denote the dielectric constant and the magnetic permeability in vacuum, respectively. One can obtain the expression for the normalization factor as

$$E_0 = \sqrt{4nP \Big/ \left\{ \pi w_0^2 n_m \varepsilon_0 c \sum_{n=1}^{N} \frac{(-1)^{2(n-1)}}{N^2} \binom{N}{n} \binom{N}{n} [(1-p^2)/(1+p^2)] \right\}} \tag{4}$$

It is well known that a partially coherent beam can be characterized by the cross-spectral density of the form [25,33,36]

$$\begin{aligned} W_N(\boldsymbol{\rho}_1, \boldsymbol{\rho}_2; z=0) &= \left\langle E_N(\boldsymbol{\rho}_1, z=0) E_N^*(\boldsymbol{\rho}_2, z=0) \right\rangle \\ &= E_0^2 \sum_{n=1}^{N} \sum_{m=1}^{N} \frac{(-1)^{n+m}}{N^2} \binom{N}{n} \binom{N}{m} \left[\exp\left(-\frac{n\boldsymbol{\rho}_1^2}{w_0^2}\right) - \exp\left(-\frac{n\boldsymbol{\rho}_1^2}{w_p^2}\right) \right] \\ &\quad \times \left[\exp\left(-\frac{m\boldsymbol{\rho}_2^2}{w_0^2}\right) - \exp\left(-\frac{m\boldsymbol{\rho}_2^2}{w_p^2}\right) \right] \exp\left[-\frac{(\boldsymbol{\rho}_1 - \boldsymbol{\rho}_2)^2}{2\sigma_0^2} \right] \end{aligned} \tag{5}$$

with σ_0 being the transverse spatial coherence width, and when $\sigma_0 \to \infty$, Equation (5) reduces to the form for a coherent DHB. After some arrangement, Equation (5) can be expressed in the following tensor form [25,33,36]

$$W_N(\boldsymbol{\rho}_1,\boldsymbol{\rho}_2;z=0)=E_0^2\sum_{n=1}^{N}\sum_{m=1}^{N}\frac{(-1)^{n+m}}{N^2}\binom{N}{n}\binom{N}{m}\times\left[\exp\left(-\tfrac{ik}{2}\tilde{\boldsymbol{\rho}}^{\mathrm{T}}\mathbf{M}_1^{-1}\tilde{\boldsymbol{\rho}}\right)-\exp\left(-\tfrac{ik}{2}\tilde{\boldsymbol{\rho}}^{\mathrm{T}}\mathbf{M}_2^{-1}\tilde{\boldsymbol{\rho}}\right)-\exp\left(-\tfrac{ik}{2}\tilde{\boldsymbol{\rho}}^{\mathrm{T}}\mathbf{M}_3^{-1}\tilde{\boldsymbol{\rho}}\right)+\exp\left(-\tfrac{ik}{2}\tilde{\boldsymbol{\rho}}^{\mathrm{T}}\mathbf{M}_4^{-1}\tilde{\boldsymbol{\rho}}\right)\right] \tag{6}$$

where $k=2\pi/\lambda$ is the wave number with λ being the wavelength of the beam, the position vector can be expressed as $\tilde{\boldsymbol{\rho}}^{\mathrm{T}}=\left(\boldsymbol{\rho}_1^{\mathrm{T}}\quad\boldsymbol{\rho}_2^{\mathrm{T}}\right)=(x_1\quad y_1\quad x_2\quad y_2)$, and $\mathbf{M}_i^{-1}$ is a 4×4 complex matrix given by

$$\mathbf{M}_1^{-1}=\begin{bmatrix}\left(-\frac{2ni}{kw_0^2}-\frac{i}{k\sigma_0^2}\right)\mathbf{I} & \frac{i}{k\sigma_0^2}\mathbf{I}\\ \frac{i}{k\sigma_0^2}\mathbf{I} & \left(-\frac{2mi}{kw_0^2}-\frac{i}{k\sigma_0^2}\right)\mathbf{I}\end{bmatrix},\quad \mathbf{M}_2^{-1}=\begin{bmatrix}\left(-\frac{2ni}{kw_p^2}-\frac{i}{k\sigma_0^2}\right)\mathbf{I} & \frac{i}{k\sigma_0^2}\mathbf{I}\\ \frac{i}{k\sigma_0^2}\mathbf{I} & \left(-\frac{2mi}{kw_0^2}-\frac{i}{k\sigma_0^2}\right)\mathbf{I}\end{bmatrix},$$
$$\mathbf{M}_3^{-1}=\begin{bmatrix}\left(-\frac{2ni}{kw_0^2}-\frac{i}{k\sigma_0^2}\right)\mathbf{I} & \frac{i}{k\sigma_0^2}\mathbf{I}\\ \frac{i}{k\sigma_0^2}\mathbf{I} & \left(-\frac{2mi}{kw_p^2}-\frac{i}{k\sigma_0^2}\right)\mathbf{I}\end{bmatrix},\quad \mathbf{M}_4^{-1}=\begin{bmatrix}\left(-\frac{2ni}{kw_p^2}-\frac{i}{k\sigma_0^2}\right)\mathbf{I} & \frac{i}{k\sigma_0^2}\mathbf{I}\\ \frac{i}{k\sigma_0^2}\mathbf{I} & \left(-\frac{2mi}{kw_p^2}-\frac{i}{k\sigma_0^2}\right)\mathbf{I}\end{bmatrix} \tag{7}$$

here, $\mathbf{I}$ is a 2×2 unit matrix. By applying the tensor *ABCD* law of partially coherent beam [41], after paraxial propagation through a general astigmatic *ABCD* optical system, the cross-spectral density of a partially coherent DHB after passing through a lens system can be expressed as [25,33,41]

$$W_N(\boldsymbol{\rho}_1,\boldsymbol{\rho}_2;z)=E_0^2\sum_{n=1}^{N}\sum_{m=1}^{N}\frac{(-1)^{n+m}}{N^2}\binom{N}{n}\binom{N}{m}\times\left\{\left[\det\left(\bar{\mathbf{A}}+\bar{\mathbf{B}}\mathbf{M}_1^{-1}\right)\right]^{-1/2}\exp\left(-\frac{ik}{2}\tilde{\boldsymbol{\rho}}^{\mathrm{T}}\mathbf{N}_1^{-1}\tilde{\boldsymbol{\rho}}\right)-\left[\det\left(\bar{\mathbf{A}}+\bar{\mathbf{B}}\mathbf{M}_2^{-1}\right)\right]^{-1/2}\exp\left(-\frac{ik}{2}\tilde{\boldsymbol{\rho}}^{\mathrm{T}}\mathbf{N}_2^{-1}\tilde{\boldsymbol{\rho}}\right)-\left[\det\left(\bar{\mathbf{A}}+\bar{\mathbf{B}}\mathbf{M}_3^{-1}\right)\right]^{-1/2}\times\exp\left(-\frac{ik}{2}\tilde{\boldsymbol{\rho}}^{\mathrm{T}}\mathbf{N}_3^{-1}\tilde{\boldsymbol{\rho}}\right)+\left[\det\left(\bar{\mathbf{A}}+\bar{\mathbf{B}}\mathbf{M}_4^{-1}\right)\right]^{-1/2}\exp\left(-\frac{ik}{2}\tilde{\boldsymbol{\rho}}^{\mathrm{T}}\mathbf{N}_4^{-1}\tilde{\boldsymbol{\rho}}\right)\right\} \tag{8}$$

where $\bar{\mathbf{A}}$, $\bar{\mathbf{B}}$, $\bar{\mathbf{C}}$, and $\bar{\mathbf{D}}$ can be defined as follows [25,41]:

$$\bar{\mathbf{A}}=\begin{bmatrix}\mathbf{A} & 0\mathbf{I}\\ 0\mathbf{I} & \mathbf{A}\end{bmatrix},\quad \bar{\mathbf{B}}=\begin{bmatrix}\mathbf{B} & 0\mathbf{I}\\ 0\mathbf{I} & -\mathbf{B}\end{bmatrix},\quad \bar{\mathbf{C}}=\begin{bmatrix}\mathbf{C} & 0\mathbf{I}\\ 0\mathbf{I} & -\mathbf{C}\end{bmatrix},\quad \bar{\mathbf{D}}=\begin{bmatrix}\mathbf{D} & 0\mathbf{I}\\ 0\mathbf{I} & \mathbf{D}\end{bmatrix} \tag{9}$$

following tensor *ABCD* law, $\mathbf{N}_i^{-1}$ and $\mathbf{M}_i^{-1}$ are related as follows [25,41]:

$$\mathbf{N}_i^{-1}=\left(\bar{\mathbf{C}}+\bar{\mathbf{D}}\mathbf{M}_i^{-1}\right)\left(\bar{\mathbf{A}}+\bar{\mathbf{B}}\mathbf{M}_i^{-1}\right)^{-1} \tag{10}$$

Now, we consider the partially coherent DHBs propagating through a lens system as shown in Figure 1, the transfer matrix of the optical system between the input plane and the output plane can be given by

$$\begin{bmatrix}\mathbf{A} & \mathbf{B}\\ \mathbf{C} & \mathbf{D}\end{bmatrix}=\begin{bmatrix}(-\Delta z/f)\mathbf{I} & (f+\Delta z)\mathbf{I}\\ (-1/f)\mathbf{I} & \mathbf{I}\end{bmatrix} \tag{11}$$

f is the focus length of the thin lens, Δz is the axial distance between the geometrical focus plane and the output plane, the output plane is located at $z=f+\Delta z$. The intensity of a partially coherent DHB at the output plane is given by

$$I(\mathbf{r},z)=n_m\varepsilon_0 cW_N(\boldsymbol{\rho},\boldsymbol{\rho};z)/2 \tag{12}$$

where $\mathbf{r}$ is the transverse position vector at the output plane.

In our calculations, we choose the following parameters: $\lambda=632.8$ nm, $f=10$ mm, the laser beam power $P_0=100$ mW, and the other beam parameters are given in each figure. We calculate in Figure 2 the evolution behavior of the intensity distribution of focused partially coherent DHBs for different values of the spatial coherence at several propagation distances in the vicinity of the focus. One can find that the focusing properties of partially coherent DHBs with small spatial coherence are quite different from that of coherent DHBs or partially coherent DHBs with large spatial coherence. For the partially coherent DHBs with small spatial coherence (see Figure 2(*a*)), the central dip of the hollow shape gradually disappears and finally evolves into a quasi-Gaussian distribution at the focal plane. However, for the coherent DHBs or partially coherent DHBs with large spatial coherence, an anomalous hollow beam with a solid core will appear in the process of focusing, and eventually, a sharp main peak with tiny side lobes will form at the focal plane $\Delta z=0$. Away from the focal plane, the

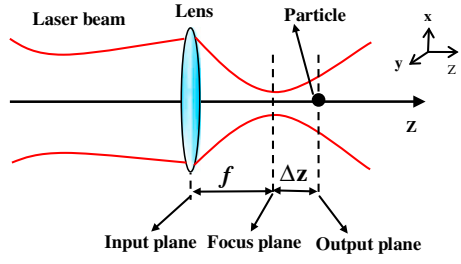

Figure 1. Schematic of the focusing optical system. (The colour version of this figure is included in the online version of the journal.)

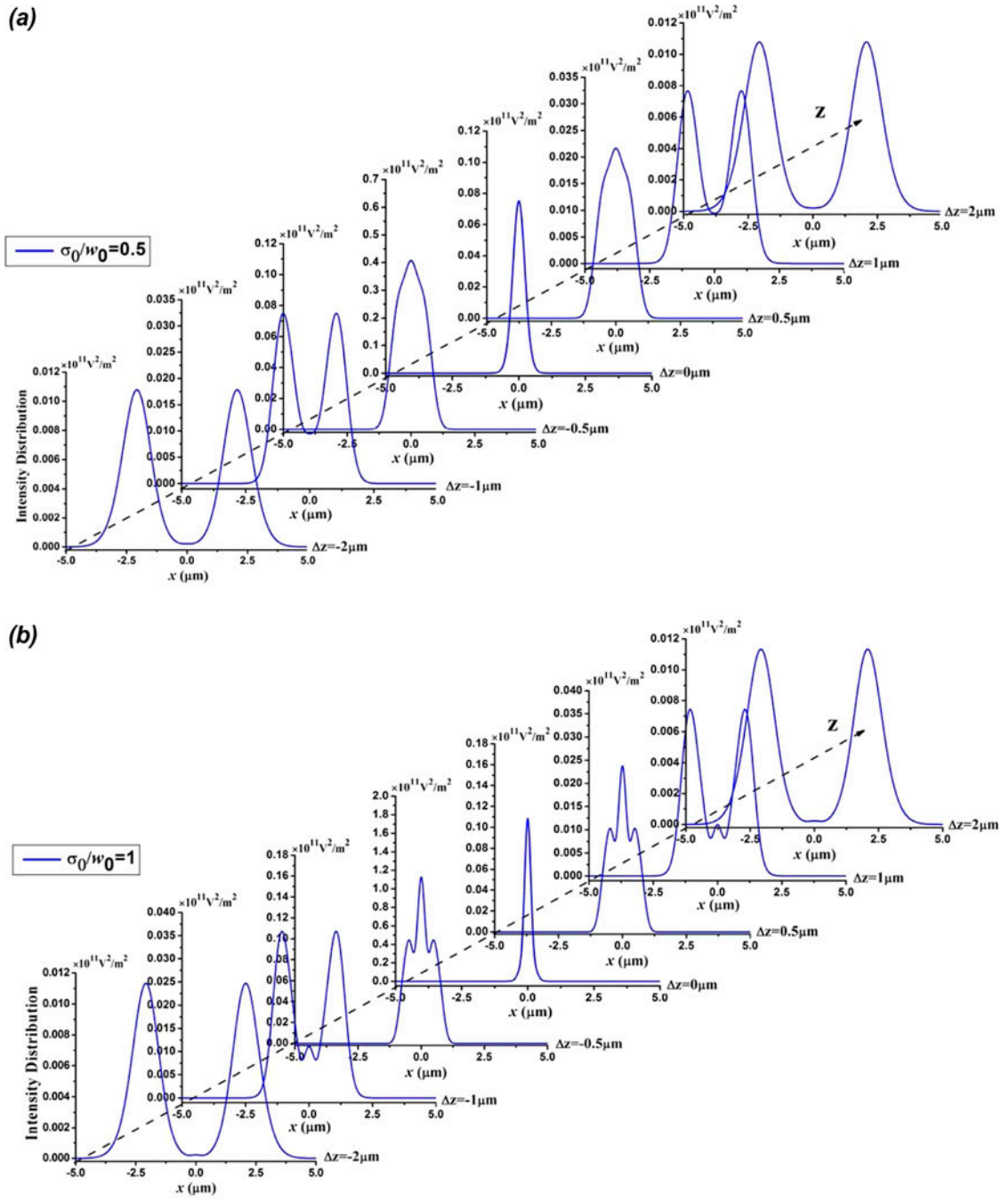

Figure 2. Evolution of intensity distribution of focused partially coherent DHBs for different values of the spatial coherence at several propagation distances in the vicinity of the focus. The other beam parameters are $N = 3$, $p = 0.6$, and $w_0 = 10$ mm. (The colour version of this figure is included in the online version of the journal.)

intensity distribution of focused partially coherent DHBs gradually evolves into a hollow shape. In addition, the DHBs with larger spatial coherence can be focused more tightly as expected [25]. Owing to these focusing characteristics, the focused coherent and partially coherent DHBs can be expected to trap particles with high refractive index. We will discuss the effect of the beam parameters of partially coherent DHBs on the RFs and the trap stiffness in detail in the following section.

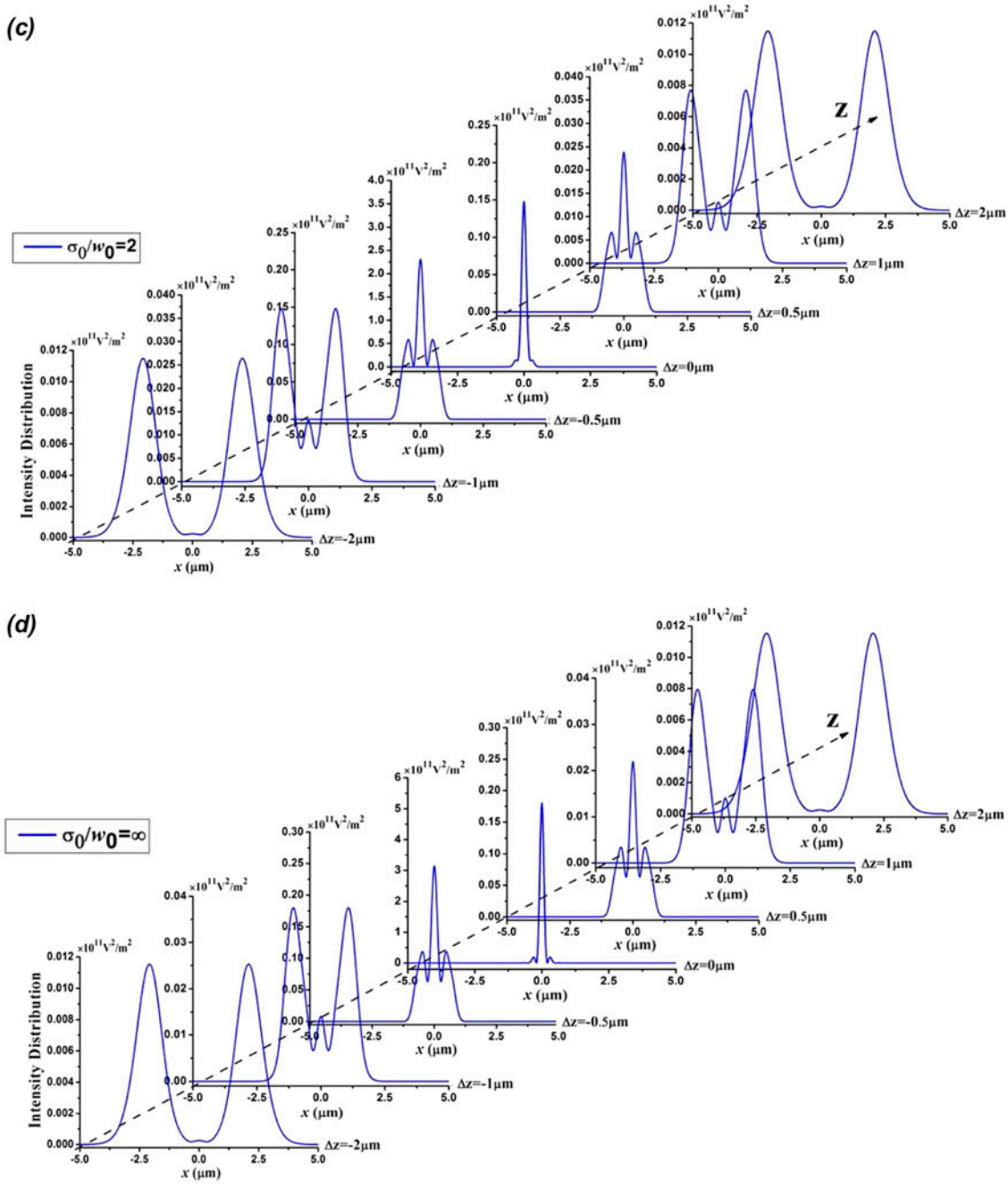

Figure 2. (*Continued*).

3. The RFs produced by focused partially coherent DHBs on a Rayleigh particle

In this section, we study the RFs produced by focused coherent and partially coherent DHBs acting on a dielectric particle in the Rayleigh regime (i.e. the radius of particle $a \ll \lambda$). Such a small dielectric particle develops an electric dipole moment in response to the instantaneous electric field, and the Rayleigh scattering model is applicable to the calculation of the RFs. The radiation pressure force exerted on the electric dipole moment can be described by two components. One component is the so-called scattering force $\boldsymbol{F}_{\mathrm{Scat}}$, which is produced due to the scattering of light by the dielectric sphere. According the Rayleigh scattering theory, the scattering force is proportional to light-intensity, and the direction goes along with the direction of the Poynting vector, and can be expressed as [10]

$$\vec{\boldsymbol{F}}_{\mathrm{Scat}}(\mathbf{r}, z) = \vec{\boldsymbol{e}}_z C_{\mathrm{pr}} I(\mathbf{r}, z) n_m / c \tag{13}$$

where $\vec{e}_z$ is a unity vector along the beam propagation, C_{pr} is the cross section of radiation pressure for the interaction between the light beam and microsphere. In the Rayleigh regime, the dielectric particle scatters the light isotropically, and C_{pr} is equal to the scattering cross section C_{Scat} which is given by [10].

$$C_{\mathrm{pr}} = C_{\mathrm{Scat}} = \frac{8}{3}\pi(ka)^4 a^2 \left[\left(\gamma^2 - 1\right)/\left(\gamma^2 + 2\right)\right]^2 \qquad (14)$$

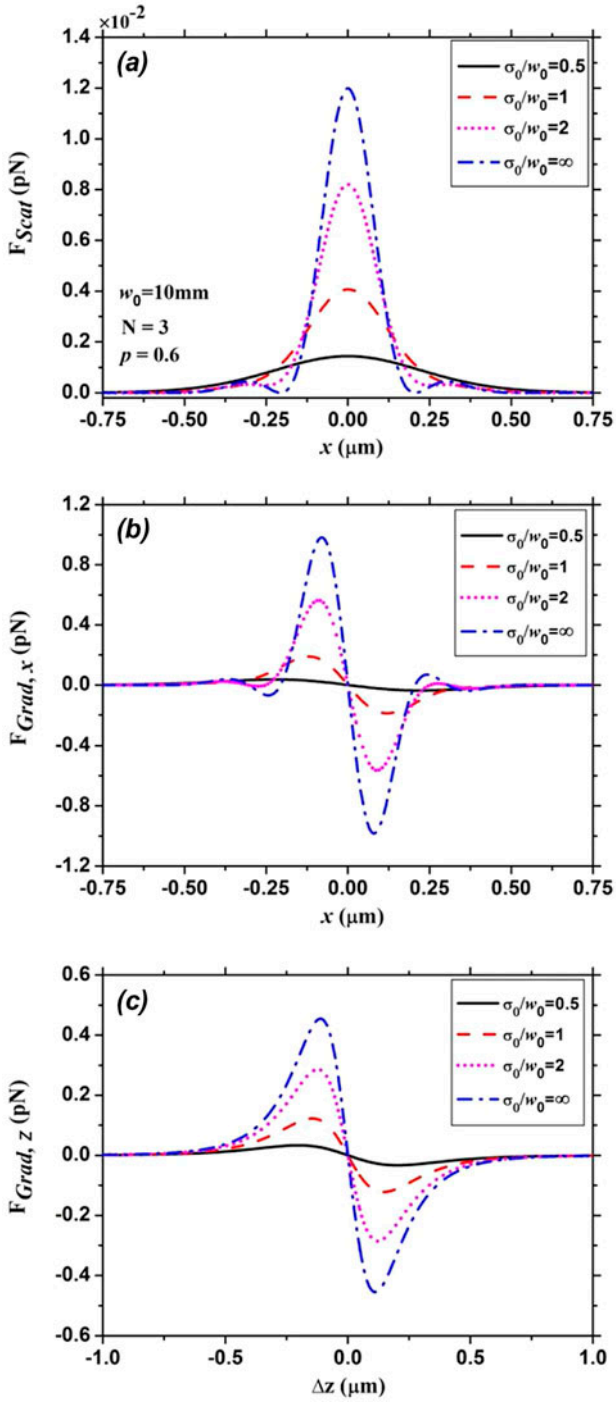

Figure 3. The RFs of partially coherent DHBs on a Rayleigh particle with $a = 40$ nm for different values of the spatial coherence σ_0/w_0. The other parameters are $N = 3$, $w_0 = 10$ mm, and $p = 0.6$. (The colour version of this figure is included in the online version of the journal.)

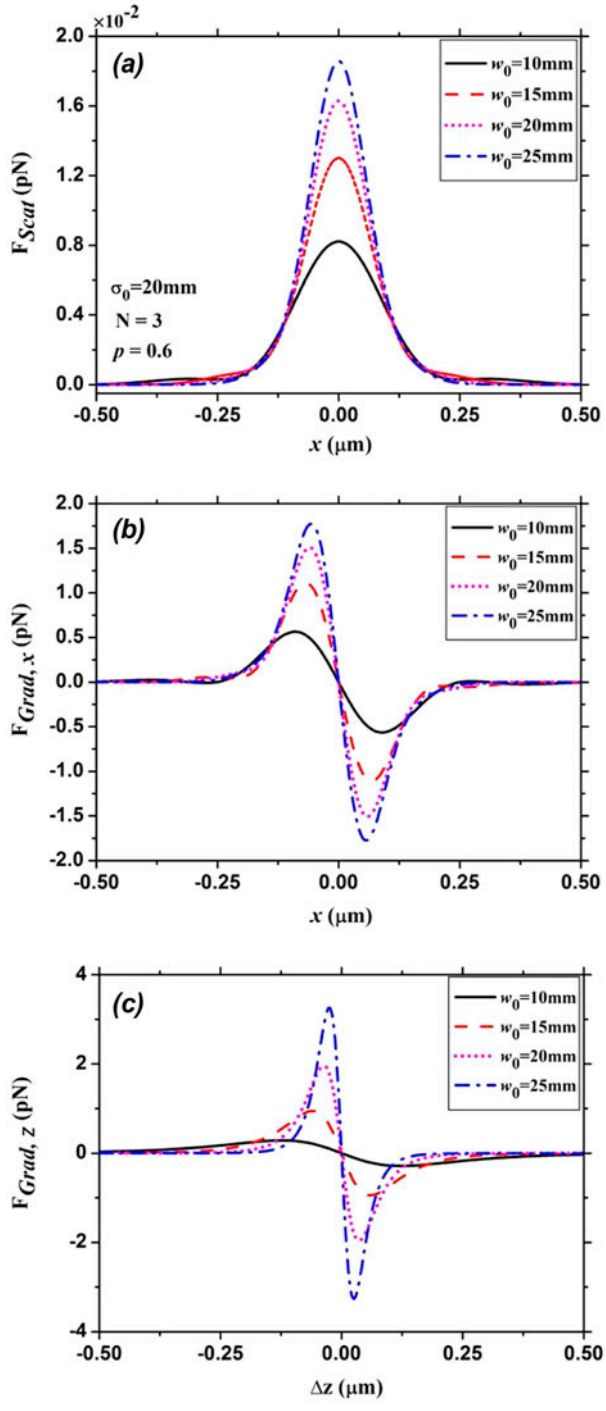

Figure 4. The RFs of partially coherent DHBs on a Rayleigh particle with $a = 40$ nm for different values of the beam waist width w_0. The other parameters are $N = 3$, $\sigma_0 = 20$ mm, and $p = 0.6$. (The colour version of this figure is included in the online version of the journal.)

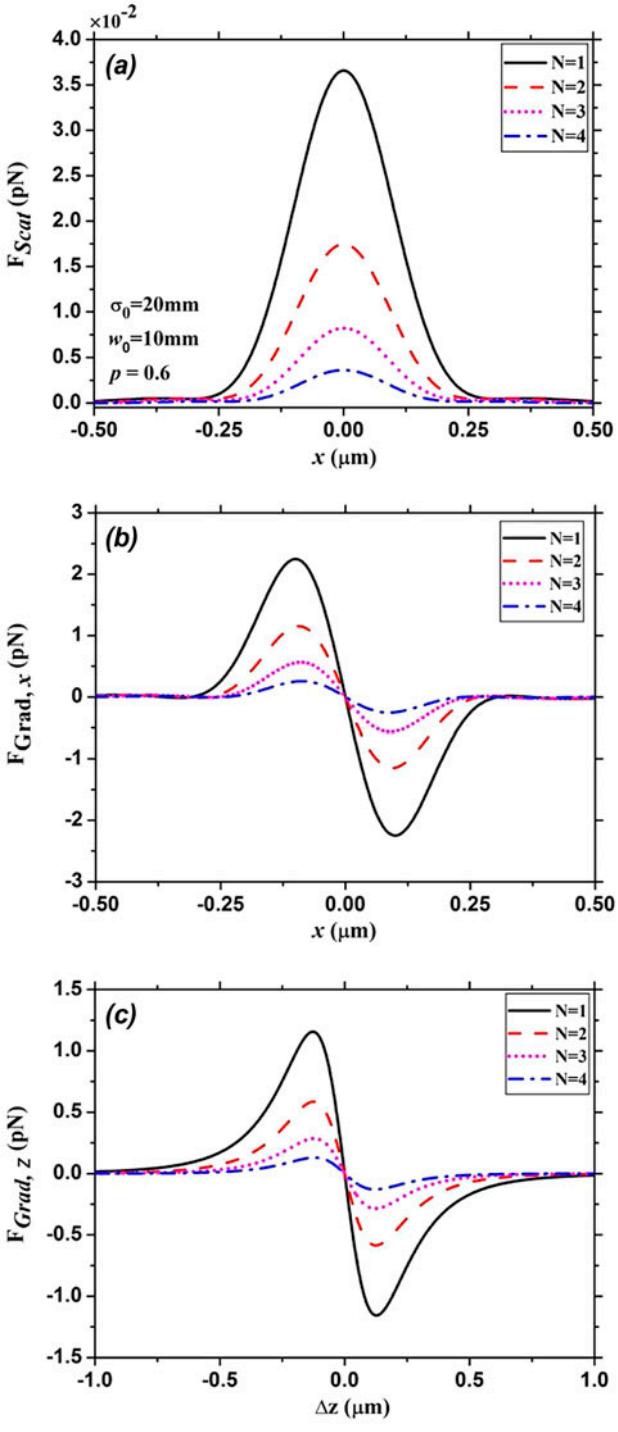

Figure 5. The RFs of partially coherent DHBs on a Rayleigh particle with $a = 40$ nm for different values of the beam order N. The other beam parameters are $\sigma_0 = 20$ mm, $w_0 = 10$ mm, and $p = 0.6$. (The colour version of this figure is included in the online version of the journal.)

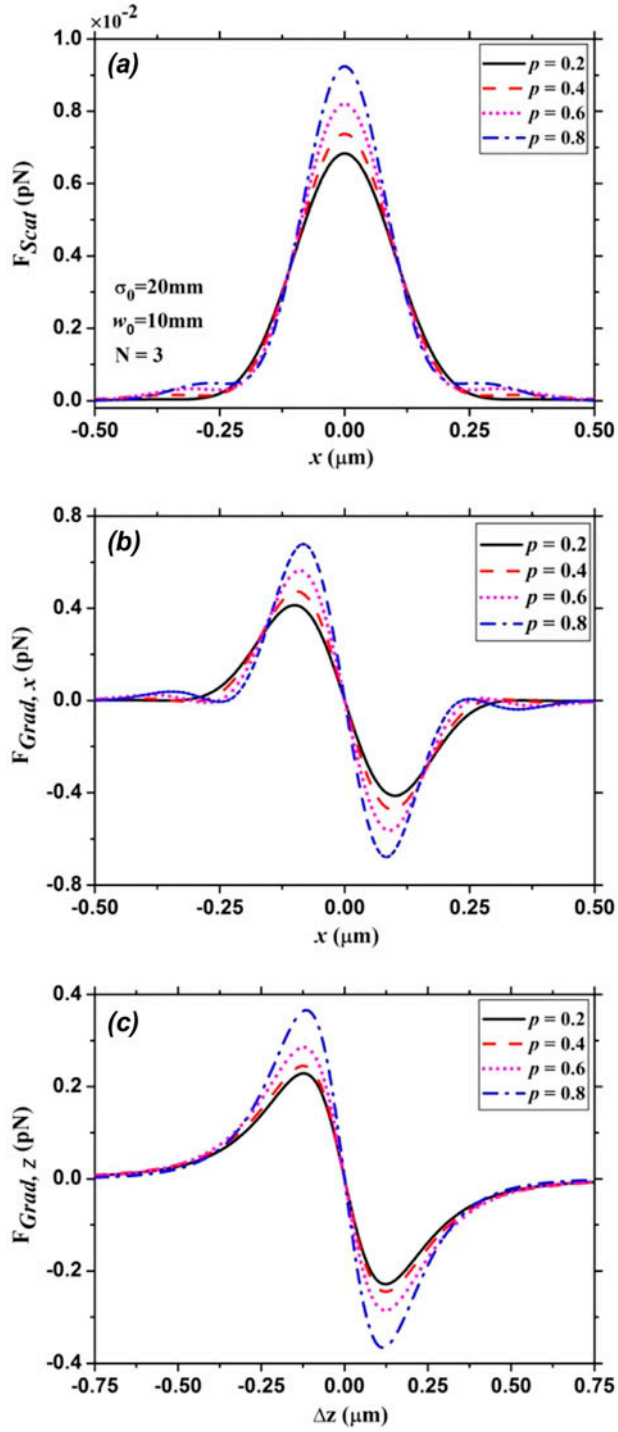

Figure 6. The RFs of partially coherent DHBs on a Rayleigh particle with $a = 40$ nm for different values of the hollow parameter p. The other beam parameters are $\sigma_0 = 20$ mm, $N = 3$, and $w_0 = 10$ mm. (The colour version of this figure is included in the online version of the journal.)

where $\gamma = n_p/n_m$ represents the relative index, n_p denotes the refractive index of the particle.

Another component of radiation pressure force is the Lorentz force induced by a nonuniform electromagnetic filed on the dipole, which is called as the gradient force $\boldsymbol{F}_{\mathrm{Grad}}$, and can be expressed as [10]

$$\vec{\boldsymbol{F}}_{\mathrm{Grad}}(\mathbf{r},z) = \frac{2\pi n_m a^3}{c}\left(\frac{\gamma^2-1}{\gamma^2+2}\right)\nabla I(\mathbf{r},z) \qquad (15)$$

Using the formulas derived above, some numerical calculations are carried out to show the RFs on a Rayleigh dielectric sphere produced by focused coherent and partially coherent DHBs. We assume the radius of the particle $a = 40$ nm, the refractive index of the particle $n_p = 1.592$ (i.e. glass) and the refractive index of the ambient $n_m = 1.332$ (i.e. water).

We calculate in Figure 3 the scattering force, the transverse gradient force and the longitudinal gradient force of focused partially coherent DHBs for different values of initial spatial coherence σ_0, respectively. As indicated by Figure 3, one can find that both the scattering and gradient forces are greatly affected by the spatial coherence. For the fully coherent beams as $\sigma_0/w_0 \to \infty$, the magnitude of the RFs is the largest; however, it will decrease as the spatial coherence decreases. Comparing the longitudinal gradient force with the forward scattering force, it is at least two orders of magnitude larger than the scattering force; thus, the scattering force can be neglected. From Figure 3(*b*) and (*c*), we can see that there is one stable equilibrium point at the focus, indicating that a Rayleigh dielectric particle whose refractive index is larger than that of the ambient (i.e. $\gamma > 1$) can be trapped by the focused coherent and partially coherent DHBs. What's more, the trapping stability can be improved by increasing the spatial coherence of the beams.

In addition, we also study the effect of the beam waist width w_0, beam order N, and hollow parameter p on the RFs as shown in Figures 4–6, respectively. As

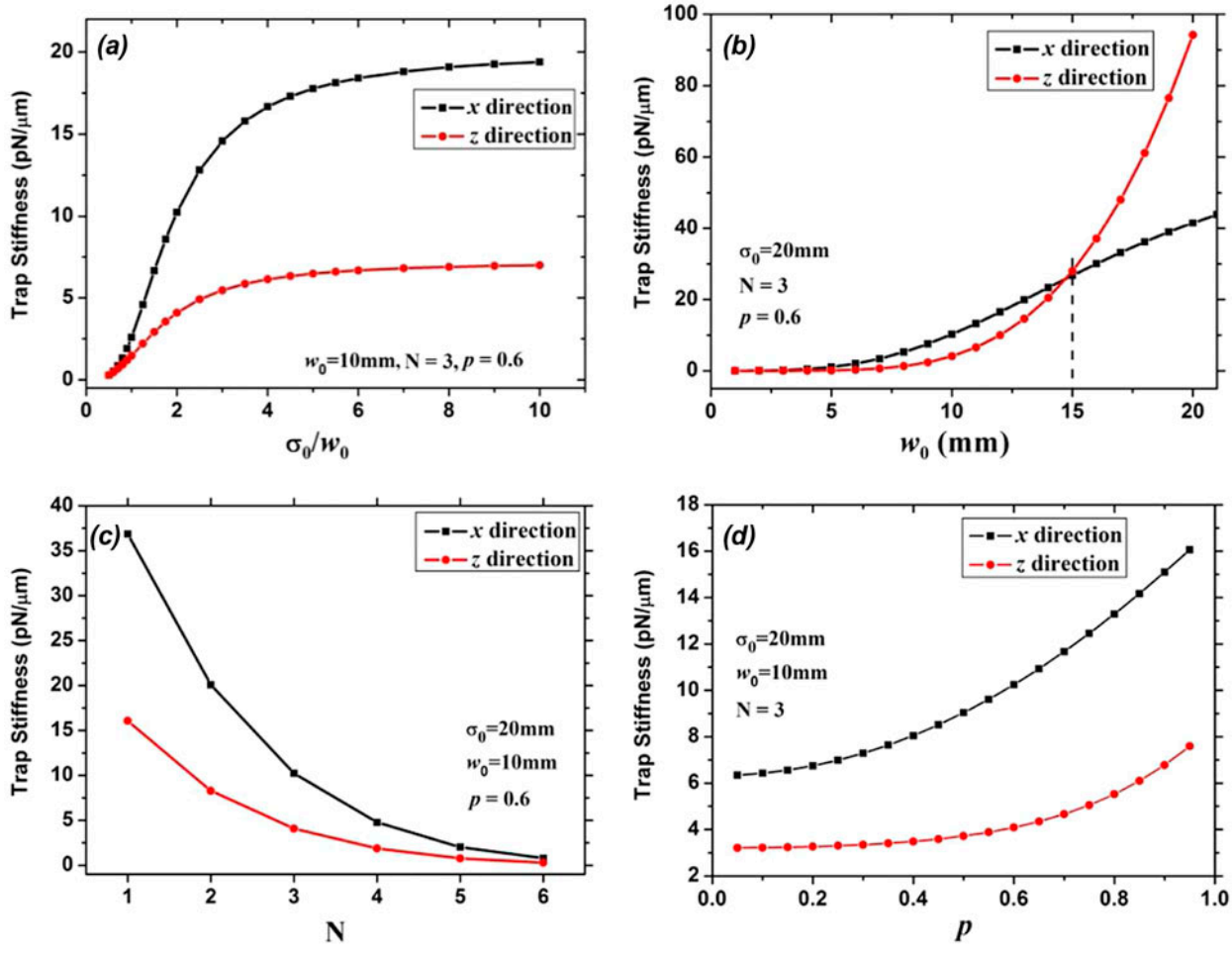

Figure 7. Dependence of the transverse and longitudinal trap stiffness on (*a*) the initial spatial coherence σ_0/w_0, (*b*) the beam waist width w_0, (*c*) the beam order N, and (*d*) the hollow parameter p. The other beam parameters are given in each figure. (The colour version of this figure is included in the online version of the journal.)

can be seen, the scattering force is always much smaller than the longitudinal gradient force and thus can be neglected. Furthermore, the magnitude of the RFs increases as w_0 or p increases, which is of benefit to trapping. However, as shown in Figure 6, both the RFs and trapping range decrease as N increases, which means that the trapping stability becomes worse for high-order beams.

In general, the trap stiffness can be used to describe the trapping stability [42], the transverse and longitudinal trap stiffness can be expressed as [20] $\kappa_x = |\partial \boldsymbol{F}_x/\partial x|_{X_{equ}}$ and $\kappa_z = |\partial \boldsymbol{F}_z/\partial z|_{Z_{equ}}$, respectively. We calculate in Figure 7 the dependence of the trap stiffness on the spatial coherence σ_0/w_0, beam waist width w_0, beam order N, and hollow parameter p of partially coherent DHBs, respectively. As indicated by Figure 7(a), both the transverse and longitudinal trap stiffness decrease as σ_0/w_0 decreases, and the transverse trap stiffness is always larger than the longitudinal trap stiffness. From Figure 7(b), we can see that both the transverse and longitudinal trap stiffness increase as w_0 increases. More interestingly, the longitudinal trap stiffness increases more rapidly as $w_0 > 15$ mm, as a result, the value of the longitudinal trap stiffness exceeds that of the transverse trap stiffness. This indicates that the partially coherent DHBs with large beam waist width are suitable for trapping, especially for the longitudinal trapping. From Figure 7(c) and (d), it is found that both the transverse and longitudinal trap stiffness increase with the decrease of N or with the increase of p. Therefore, one comes to the conclusion that we can use partially coherent DHBs with larger spatial coherence, larger waist width, smaller beam order, and larger hollow parameter to enhance the trap stiffness, and thus to improve the trapping capability.

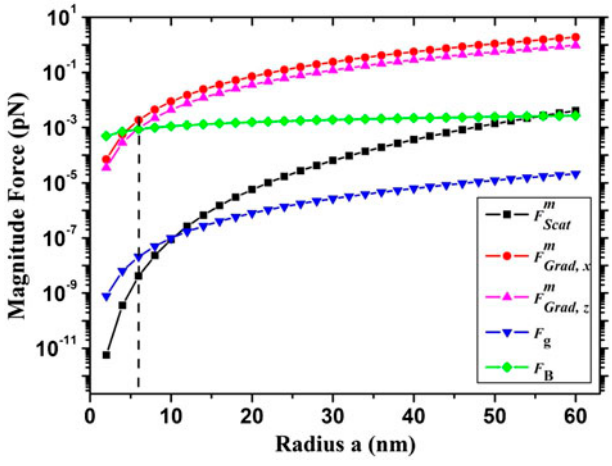

Figure 8. Dependence of $\boldsymbol{F}^m_{\mathrm{Scat}}$, $\boldsymbol{F}^m_{\mathrm{Grad},x}$, $\boldsymbol{F}^m_{\mathrm{Grad},z}$, $\boldsymbol{F}_g$ and $\boldsymbol{F}_B$ on particle radius a, the beam parameters are $N = 3$, $\sigma_0 = 20$ mm, $w_0 = 10$ mm, and $p = 0.6$. (The colour version of this figure is included in the online version of the journal.)

4. Analysis of trapping stability

In order to stably trap and manipulate the particles, the longitudinal gradient force should be large enough to overcome the forward scattering force, i.e. $R = |\boldsymbol{F}_{\mathrm{Grad},z}|/|\boldsymbol{F}_{\mathrm{Scat}}| > 1$, where the ratio R is called stability criterion. Obviously, from Figures 3 to 6, we can see that the magnitude of the scattering force is much smaller than the gradient force, and thus, this stability criterion can be easily satisfied. In addition, for very small particles, the disturbance from the Brownian motion due to the thermal fluctuation from the ambient (i.e. water) will strongly affect the trapping stability. According to the fluctuation–dissipation theorem of Einstein, the magnitude of the Brownian force can be calculated by [43] $|\boldsymbol{F}_B| = \sqrt{12\pi\eta a k_B T}$, where the viscosity for water $\eta = 7.977 \times 10^{-4}$ Pa s at the room temperature of $T = 300$ K, k_B is the Boltzmann constant.

For the convenience of comparison, we plot in Figure 8 the change of the magnitude of all the forces, including the maximum scattering force $\boldsymbol{F}^m_{\mathrm{Scat}}$, the maximum transverse gradient force $\boldsymbol{F}^m_{\mathrm{Grad},x}$, the maximum longitudinal gradient force $\boldsymbol{F}^m_{\mathrm{Grad},z}$, the Brownian force $\boldsymbol{F}_B$, and the gravity $\boldsymbol{F}_g$, versus the radius of particle. It is evident from Figure 8 that the gravity of the particle can be ignored comparing with the RFs. As is shown in Figure 8, when the particle is very small (in our case, $a < 6$ nm), the gradient forces are smaller than the Brownian force, making the Brownian force dominant. Thus, it is not suitable to trap too small particles. For large particles, the scattering force becomes dominant and plays a crucial role on the trapping stability (not show here). What's more, trapping for very large particles is beyond the theory of Rayleigh approximation, in this case, the T-matrix method or the ray optical model should be applied to calculate the optical force.

5. Conclusions

In conclusion, we have theoretically and numerically studied the evolution behavior of intensity distribution of focused coherent and partially coherent DHBs in the vicinity of the focus, and we have found that the focusing properties of partially coherent DHBs are closely related to their spatial coherence. In addition, we have also investigated the RFs of focused coherent and partially coherent DHBs on a Rayleigh dielectric particle. Our results have shown that the focused coherent and partially coherent DHBs can be focused into a tight focal spot, which can be used to stably trap and manipulate the particles with high refractive index at the focal point.

Of particular interest is that both the RFs and trap stiffness increase with the increase of the spatial coherence, beam waist width, and hollow parameter or with the decrease of beam order, which is of benefit to trapping. Finally, the stability conditions for effective trapping particles have been analyzed. Our results are interesting and useful for experimental particle trapping by means of optical tweezers.

Acknowledgements

Acknowledgement is made to the Thousand Youth Talents Plan.

Disclosure statement

No potential conflict of interest was reported by the authors.

Funding

This work is supported by the National Natural Science Foundation of China (NSFC) [grant number 21133008], [grant number 11374015].

References

[1] Ashkin, A.; Dziedzic, J.M.; Bjorkholm, J.E.; Chu, S. *Opt. Lett.* **1986,** *11*, 288–290.
[2] Zhan, Q. *Opt. Express* **2004,** *12*, 3377–3382.
[3] Min, C.; Shen, Z.; Shen, J.; Zhang, Y.; Fang, H.; Yuan, G.; Du, L.; Zhu, S.; Lei, T.; Yuan, X. *Nat. Commun.* **2013,** *4*, 2891.
[4] Chu, S.; Bjorkholm, J.E.; Ashkin, A.; Cable, A. *Phys. Rev. Lett.* **1986,** *57*, 314–317.
[5] Mitchem, L.; Reid, J.P. *Chem. Soc. Rev.* **2008,** *37*, 756–769.
[6] Dear, R.D.; Burnham, D.R.; Summers, M.; McGloin, D.; Ritchie, G. *Phys. Chem. Chem. Phys.* **2012,** *14*, 15826–15831.
[7] Oroszi, L.; Galajda, P.; Kirei, H.; Bottka, S.; Ormos, P. *Phys. Rev. Lett.* **2006,** *97*, 058301.
[8] Zhong, M.; Wei, X.; Zhou, J.; Wang, Z.; Li, Y. *Nat. Commun.* **2013,** *4*, 1768.
[9] Grier, D.G. *Nature* **2003,** *424*, 810–816.
[10] Harada, Y.; Asakura, T. *Opt. Commun.* **1996,** *124*, 529–541.
[11] Kawauchi, H.; Yonezawa, K.; Kozawa, Y.; Sato, S. *Opt. Lett.* **2007,** *32*, 1839–1841.
[12] Yan, S.; Yao, B. *Phys. Rev. A* **2007,** *76*, 053836.
[13] Yan, S.; Yao, B. *J. Opt. Soc. Am. B* **2007,** *24*, 1596–1602.
[14] Liu, Z.; Zhao, D. *Opt. Express* **2012,** *20*, 2895–2904.
[15] Wang, L.; Zhao, C. *Opt. Express* **2007,** *15*, 10615–10621.
[16] Jiang, Y.; Huang, K.; Lu, X. *Opt. Express* **2011,** *19*, 9708–9713.
[17] Jiang, Y.; Huang, K.; Lu, X. *Opt. Express* **2013,** *21*, 24413–24421.
[18] Wang, L. *Opt. Express* **2012,** *20*, 20814–20826.
[19] Zhang, Y.; Ding, B.; Suyama, T. *Phys. Rev. A* **2010,** *81*, 023831.
[20] Zhang, Y.; Suyama, T.; Ding, B. *Opt. Lett.* **2010,** *35*, 1281–1283.
[21] Liu, Z.; Zhao, D. *Appl. Opt.* **2013,** *52*, 1310–1316.
[22] Mandel, L.; Wolf, E. *Optical Coherence and Quantum Optics;* Cambridge University Press: Cambridge, 1995.
[23] Wu, J.; Boardman, A.D. *J. Mod. Opt.* **1991,** *38*, 1355–1363.
[24] Wang, L.; Zhao, C.; Wang, L.; Lu, X.; Zhu, S. *Opt. Lett.* **2007,** *32*, 1393–1395.
[25] Zhao, C.; Cai, Y.; Lu, X.; Eyyuboğlu, H. *Opt. Express* **2009,** *17*, 1753–1765.
[26] Zhao, C.; Cai, Y. *Opt. Lett.* **2011,** *36*, 2251–2253.
[27] Dong, Y.; Wang, F.; Zhao, C.; Cai, Y. *Phys. Rev. A* **2012,** *86*, 013840.
[28] Shu, J.; Chen, Z.; Pu, J. *J. Opt. Soc. Am. A* **2013,** *30*, 916–922.
[29] Yin, J.; Zhu, Y.; Wang, W.; Wang, Y.; Jhe, W. *J. Opt. Soc. Am. B* **1998,** *15*, 25–33.
[30] Zhao, C.; Cai, Y.; Wang, F.; Lu, X.; Wang, Y. *Opt. Lett.* **2008,** *33*, 1389–1391.
[31] Liu, Z.; Zhao, H.; Liu, J.; Lin, J.; Ahmad, M.A.; Liu, S. *Opt. Lett.* **2007,** *32*, 2076–2078.
[32] Cai, Y.; Lu, X.; Lin, Q. *Opt. Lett.* **2003,** *28*, 1084–1086.
[33] Cai, Y.; Zhang, L. *J. Opt. Soc. Am. B* **2006,** *23*, 1398–1407.
[34] Mei, Z.; Zhao, D. *J. Opt. Soc. Am. A* **2005,** *22*, 1898–1902.
[35] Cai, Y.; He, S. *Opt. Express* **2006,** *14*, 1353–1367.
[36] Yuan, Y.; Cai, Y.; Qu, J.; Eyyuboğlu, H.; Baykal, Y.; Korotkova, O. *Opt. Express* **2009,** *17*, 17344–17356.
[37] Eyyuboğlu, H.T. *Opt. Laser Technol.* **2008,** *40*, 156–166.
[38] Cai, T.; Eyyuboğlu, H.; Baykal, Y. *Opt. Lasers Eng.* **2010,** *48*, 1019–1026.
[39] Dong, Y.; Cai, Y.; Zhao, C. *Appl. Phys. B* **2011,** *105*, 405–414.
[40] Jeffries, G.D.; Edgar, J.S.; Zhao, Y.; Shelby, J.P.; Fong, C.; Chiu, D.T. *Nano. Lett.* **2007,** *7*, 415–420.
[41] Lin, Q.; Cai, Y. *Opt. Lett.* **2002,** *27*, 216–218.
[42] Neuman, K.C.; Block, S.M. *Rev. Sci. Instrum.* **2004,** *75*, 2787–2809.
[43] Okamoto, K.; Kawata, S. *Phys. Rev. Lett.* **1999,** *83*, 4534–4537.